THE JOURNAL OF PHYSICAL CHEMISTRY C

Article

pubs.acs.org/JPCC

Imidazole-Doped Cellulose as Membrane for Fuel Cells: Structural and Dynamic Insights from Solid-State NMR

Li Zhao,[†,‡] Iga Smolarkiewicz,[†,§,∥] Hans-Heinrich Limbach,[†,#] Hergen Breitzke,[‡] Katarzyna Pogorzelec-Glaser,[§] Radosław Pankiewicz,[⊥] Jadwiga Tritt-Goc,[*,§] Torsten Gutmann,[*,‡] and Gerd Buntkowsky[*,‡]

[‡]Eduard-Zintl-Institute für Inorganic Chemistry and Physical Chemistry, Technische Universität Darmstadt, Alarich-Weiss-Str. 4, 64287 Darmstadt, Germany

[§]Institute of Molecular Physics, Polish Academy of Sciences, M. Smoluchowskiego 17, 60-179 Poznań, Poland

[∥]NanoBioMedical Centre, Adam Mickiewicz University in Poznań, Umultowska 85, 61-614 Poznan, Poland

[⊥]Faculty of Chemistry, Adam Mickiewicz University in Poznań, Umultowska 89b, 61-614 Poznań, Poland

[#]Institut für Chemie und Biochemie, Freie Universität Berlin Takustr. 3, 14195 Berlin, Germany

Supporting Information

ABSTRACT: The structure and proton tautomerism of imidazole-doped cellulose (Cell-Im), an excellent solid state proton conductor, has been studied by ^{15}N solid-state NMR techniques. $^{1}H-^{15}N$ HETCOR NMR experiments allowed us to assign the water and cellulose−OH resonances and to establish $^{1}H-^{15}N$ connectivities. ^{15}N CPMAS NMR experiments showed that imidazole is immobile and its tautomerism quenched below 263 K, whereas at higher temperatures, a broad distribution of slow and fast exchanging protons is observed, where the fraction of the latter increases with temperature. The tautomerism is found to be coupled to proton exchange with water molecules. From an analysis of the temperature-dependent fractions of both phases, a broad distribution of energies of activation of the tautomerization of Cell-Im is obtained, exhibiting a maximum at 42 kJ mol^{-1} and a width of 8.2 kJ mol^{-1}. The tautomerization is slower than in the case of imidazole dissolved in wet organic solvents. These results indicate that imidazole is located in an aqueous fluid phase between cellulose microfibrils, where proton exchange is assisted by a fast molecular reorientation in transient hydrogen-bonded imidazole−water complexes. The implications of these findings for the mechanism of proton conductivity of Cell-Im are discussed. Finally, the potential of Dynamic Nuclear Polarization (DNP) enhanced ^{15}N-natural abundance CP-MAS NMR of these heterocyclic systems is evaluated.

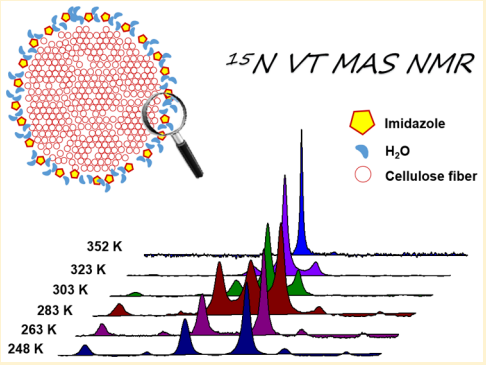

INTRODUCTION

In times of increasing energy requirement and global warming, new innovations such as fuel cells have been promoted to transform energy in an efficient and clean way.[1−5] In particular, the successful development of proton exchange membrane fuel cells (PEMFCs) has gained widespread interest.[6−9] The energy in such PEMFCs is generated by reaction of hydrogen, which is oxidized at the anode. During this reaction, protons are transferred to the cathode through a proton exchange membrane (PEM), while the electrons pass through the external circuit and induce electrical energy. One of the challenges is, therefore, to find an appropriate insulating film to separate anode and cathode material but, at the same time, to allow fast proton transport.

In the last decades, several types of polymeric materials with high proton conductivity have been reported and used. For example, polymers containing poly(tetrafluoroethylene) backbones with different anion-terminated side chains such as NAFION have been developed.[10−12] However, these materials exhibited a high proton conductivity only when they are hydrated, which limits the operation temperature of the device to about 353 K. Additionally, NAFION is quite expensive.[13] Consequently, intensive research has been done aimed at the development of cheaper and environmentally friendlier materials for membranes that can operate also under anhydrous conditions and at temperatures above 373 K. In particular, polymer backbones have been doped with heterocyclic nitrogen containing compounds, leading to solid state proton conductors, which allow one to achieve temperatures up to 473 K.[14,15] Important examples are imidazole and benzimidazole containing PEM materials, which exhibit high proton conductivities after doping with acids.[16,17] Furthermore,

Received: July 14, 2016
Revised: August 19, 2016
Published: August 22, 2016

ACS Publications © 2016 American Chemical Society

DOI: 10.1021/acs.jpcc.6b07049
J. Phys. Chem. C 2016, 120, 19574−19585

Scheme 1. Chemical Structure of Cellulose Chains[a]

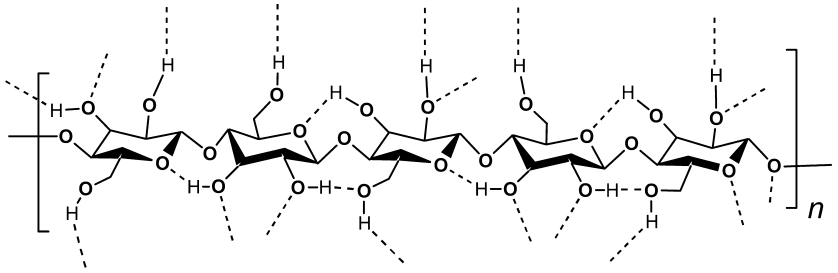

[a]The structure was designed according to ref 34.

extensive work focused on the development of biopolymer carrier materials, such as chitin and alginic acid, which contain acid groups, as well as cellulose or derivatives of cellulose that are doped with N-heterocyclic molecules, such as imidazole, benzimidazole, and pyrazole and added acids.[18−24] As PEM are generally disordered, special techniques need to be applied to obtain information about their structure and, hence, their function. These include small-angle X-ray scattering (SAXS), neutron imaging,[25−31] and vibrational spectroscopy.

Recently, by some of us, an environmentally friendly polymeric material consisting of microcrystalline cellulose (Cell) doped with neutral imidazole (Im) has been synthesized and studied, which shows a high conductivity as well as a high stability even at 433 K.[21] Cellulose is a linear polysaccharide in which the anhydroglucose repeat units are linked together through β-1,4 glycosidic bonds, as illustrated in Scheme 1. The OH groups can form both intrachain and interchain hydrogen bonds,[32] leading to complex assemblies containing dense crystalline and less dense amorphous regions.[33] Water and other small molecules can penetrate into the latter regions, but not into the former ones.

As the solid state proton tautomerism of pure imidazole is quenched,[35] the question arises how imidazole is embedded in cellulose so that proton transfer and proton conductivity are activated. Here, we have tackled this problem using high-resolution solid state NMR. In particular, ^{15}N NMR under conditions of ^{1}H−^{15}N cross-polarization (CP) and magic angle spinning (MAS) has shown to be a very valuable tool to follow multiple proton transfers from and to nitrogen in the millisecond to picosecond time scale. Proton conducting solids have been studied using various NMR techniques,[25,27,29,36−40] also in combination with other methods. For example, Schmidt-Rohr et al. developed a proton transport model for NAFION-based PEM systems, based on the tubular structure of the polymer material.[25] NMR techniques have been applied in particular to understand proton transport phenomena promoted by histidine in biomolecules such as the M2 protein.[28,31,41−43] Li and co-workers employed solid-state ^{1}H−^{13}C/^{15}N correlation spectroscopy to explain the protonation, tautomerization, and the rotameric structure of histidine at different pH conditions.[42] Recently, it has been shown by ^{15}N NMR that a very fast tautomerism of ^{15}N-labeled 4-methylimidazole in organic solvents as well as in the active site of Human Carbonic Anhydrase is activated by few water molecules.[41]

Although nanocellulose materials have been studied using solid state NMR in the last few decades,[44−46] the structure determination of doped molecules on the cellulose surface still constitutes a challenge, particularly due to their low concentrations and the low sensitivity of probe nuclei such as ^{13}C and ^{15}N at natural abundance. To overcome this issue, radicals such as TOTAPOL (Scheme 2)[47] have been embedded

Scheme 2. Chemical Structure of TOTAPOL (4-[2-Hydroxy-3-[(2,2,6,6-tetramethyl-1-oxy-4-piperidinyl)amino]propoxy]-2,2,6,6-tetramethyl-1-piperidinyloxy)[47]

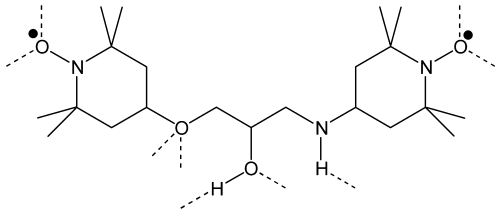

in solid samples, which is assisted by hydrogen bond formation to the matrix. The addition of radicals enables solid-state dynamic nuclear polarization (DNP).[48] The latter allows one to transfer electron polarization to nuclei of interest, which leads to strong signal enhancements. Mostly polarization is transferred to the ^{1}H from which it is conveniently transferred to heteronuclei via cross-polarization (CP). This method has also been applied very recently to study cellulose surface chemistry.[49−51]

In the present study, temperature-dependent ^{15}N CPMAS NMR and ^{1}H−^{15}N HETCOR experiments have been performed to determine whether imidazole in cell-induced is able to exchange protons with cellulose−OH groups and with residual water molecules.

In addition, we have applied ^{13}C and ^{15}N CPMAS NMR in combination with DNP-enhanced solid state experiments for the investigation of the structure, in particular, the hydrogen bond interactions of imidazole in samples of Cell-Im. In the following, after an Experimental Section, the results of these studies are presented and discussed.

EXPERIMENTAL SECTION

Sample Preparation. *General.* Microcrystalline cellulose was purchased from Sigma-Aldrich, exhibiting a relative molecular mass M_n of 74000, an average particle size of 20 μm, a degree of polymerization of about 230, and a crystallinity index of 66%. Imidazole-^{15}N and imidazole were purchased also from Sigma-Aldrich.

Cell-Im-^{15}N. For variable-temperature ^{15}N CPMAS NMR and ^{1}H−^{15}N HETCOR experiments, Cell-Im-^{15}N samples were prepared as follows. A total of 0.196 g (2.8 mmol) imidazole-^{15}N was dissolved in 20 mL of chloroform

DOI: 10.1021/acs.jpcc.6b07049
J. Phys. Chem. C 2016, 120, 19574−19585

($CHCl_3$) and 0.5 g of microcrystalline cellulose was added upon vigorous stirring. The stirring was continued at room temperature for 1 h, and the suspension afterward was ultrasonicated for 1 h at 303 K. Finally, the suspension was filtered off under reduced pressure. The residue in the glass frit was well rinsed using a large amount of chloroform and dried at 313 K for 2 h. Finally, about 0.5 g of white powder of cellulose doped with imidazole-^{15}N was obtained. An SEM image of imidazole-doped microcrystalline cellulose (Cell-Im) is depicted in Figure S1 (Supporting Information, SI). As the imidazole cannot penetrate cellulose fibers, but only adhere to their surface, the maximum amount of imidazole in the resulting Cell-Im is limited. On the basis of elemental analysis, the concentration of imidazole in the final product Cell-Im was only 1.0 mM/g, corresponding to a molar cellulose−monomer/imidazole ratio of about 4.6.[21] The initial water content of Cell-Im samples is about 3% (m%).[21] The water is introduced via the chloroform, whose water content at room temperature is around 0.1%.[52]

Im-^{15}N. As reference sample for comparison, solid imidazole-^{15}N was purchased from Aldrich. This sample was hygroscopic and contained some water.

Cell-Im-TOT. Samples for ^{15}N DNP CPMAS NMR (Cell-Im-TOT) were prepared in a similar way using nonlabeled imidazole. Each sample (25−30 mg) was impregnated with 15 μL of a 15 mM TOTAPOL solution (Dynupol, U.S.A.) in glycerol-d_8/D_2O/H_2O (60/30/10, v%).

Im-TOT. For DNP measurements, also a sample of water containing nonlabeled imidazole was prepared as follows. A total of 25 mg solid imidazole (molar ratio of Im/water about 1:1) were impregnated with 15 mL of a 15 mM TOTAPOL solution.

Variable Temperature ^{15}N CPMAS and ^{1}H−^{15}N HETCOR CPMAS Measurements. Variable temperature ^{15}N CPMAS spectra were measured on a 14.1 T Bruker AVANCE III HD spectrometer corresponding to a ^{15}N frequency of 60.82 MHz, employing a 4 mm probe and a MAS frequency of 7.5 kHz. The recycle delay and contact time was set 10 s and 3.5 ms, respectively, and 800−5616 accumulations were performed.

2D ^{1}H−^{15}N heteronuclear correlation (HETCOR) experiments were carried out with Lee−Goldburg (LG)[53] decoupling at a spinning rate of 7.5 kHz. Two different CP contact times were used in the ^{1}H−^{15}N HETCOR experiments: (i) a short contact time of 0.8 ms (not shown), similar to ref 42, to exclude couplings to remote protons and (ii) a longer contact time of 1.4 ms to be sensitive to larger distances. Except for the better S/N of the 1.4 ms spectrum, there were no substantial differences between the spectra. ^{1}H homonuclear decoupling during the t_1 dimension was achieved using the FSLG pulse sequence with a transverse ^{1}H field strength of 100 kHz.[54]

^{13}C and ^{15}N DNP CPMAS NMR Measurements. ^{13}C and ^{15}N DNP CPMAS NMR measurements were performed using a commercial 9.4 T Bruker AVANCE III spectrometer containing a 263 GHz gyrotron system, a transmission line, and a 3.2 mm Bruker ^{1}H/X/Y triple-resonance low temperature probe. For that purpose, 3.2 mm sapphire rotors were used closed with a zirconia drive cap. Using this setup, irradiation with microwaves creates ^{1}H dynamic nuclear polarization (DNP), which is then transferred via CP to ^{13}C or ^{15}N. Spectra were recorded at nominally 105 K, at frequencies of 100.59 MHz for ^{13}C and 40.53 for ^{15}N.

T_1 saturation recovery measurements were performed under microwave irradiation in order to estimate the optimum recycle delay (d1 = 1.3·T_1) for the following CPMAS experiments.[55] All CPMAS spectra with and without microwave irradiation were acquired at a spinning rate of 7.5 kHz at sample temperatures of 105 K. The CP condition was optimized with a linear ramp (75−100%).[56] The ^{13}C DNP CPMAS spectra were then measured using 16 transients with a recycle delay of 5 s and 2 ms contact time. The ^{15}N DNP CPMAS spectra were recorded using 2000−3200 scans, employing a recycle delay of 5 s and a contact time of 3 ms, respectively.

Chemical Shift Referencing. The ^{13}C and ^{15}N NMR spectra and chemical shifts reported were referenced to solid TSP ($Si(CH_3)_3$-CD_2-CD_2-COO^-Na^+) and to liquid ammonia at 25 °C, respectively. Initially, the CO group signal of solid glycine, which resonates at 176 ppm,[57] was used for the calibration of the ^{13}C. The initial reference for the ^{15}N NMR spectra was either solid $^{15}NH_4Cl$ or solid glycine-^{15}N. According to Bertani et al.[58] the corresponding values for $^{15}NH_4Cl$ and for solid glycine-^{15}N are 39.3 and 33.4 ppm, respectively, with respect to liquid ammonia at 298 K.

Whereas one-dimensional ^{1}H MAS NMR spectra can be referenced to solid TSP, it is difficult to reference the ^{1}H dimension of HETCOR spectra because of chemical shift scaling. Therefore, it has been proposed to use [U−^{13}C]L-Tyr·HCl as reference standard whose ^{1}H chemical shifts have been well established, providing a way to scale the ^{1}H dimension,[59] using the −COOH signal at 12.9 ppm and the −OH signal at 10.2 ppm.

RESULTS AND DISCUSSION

A. Structure and Dynamics of Imidazole-Doped Cellulose. *Results.* In this section we report the results of our ^{15}N and ^{1}H solid-state NMR experiments. All relevant chemical shifts are assembled in Table S1.

Variable Temperature ^{15}N CPMAS NMR Spectroscopy of Cell-Im-^{15}N. In order to obtain information about the tautomerism of imidazole in cellulose we performed ^{15}N CPMAS NMR experiments of Cell-Im-^{15}N in the temperature range between 243 and 353 K. This range is still well below the imidazole melting point at 364 K.[60] Some typical spectra are depicted in Figure 1. The spectral width was chosen to

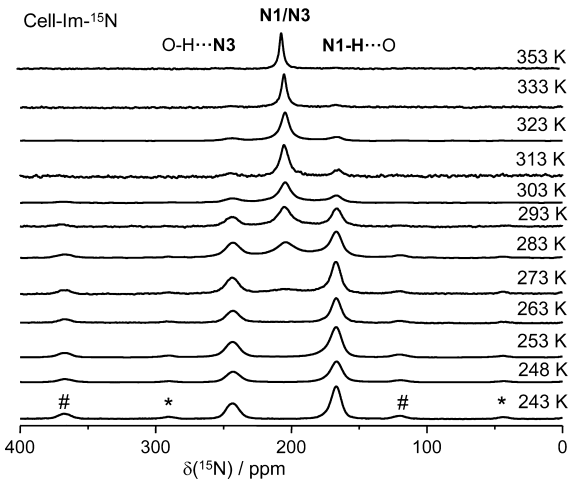

Figure 1. Temperature-dependent ^{15}N CPMAS spectra of Cell-Im-^{15}N recorded at 14.1 T and at a spinning rate of 7.5 kHz. The imino spinning side bands are marked by the symbol "#" and the amino side bands by "*".

DOI: 10.1021/acs.jpcc.6b07049
J. Phys. Chem. C 2016, 120, 19574−19585

highlight the behavior of the spinning side bands of the imino and the amino nitrogen signals, characterized by the symbols "#" and "*", respectively.

The 243 K spectrum is similar to the one at 105 K, and no major changes of the line widths are observed. This indicates a distribution of chemical shifts as expected for a disordered solid. Moreover, the distinct low-field imino and the high-field amino signals indicate slow proton exchange. The spinning sidebands show that the rotational diffusion of the imidazole molecules is slow at 243 K.

Interestingly, at 273 K, centered between the low-temperature imino and amino signals, a new signal appears which clearly corresponds to fast exchanging imidazole amino/imino nitrogens. While this signal is significantly visible at temperatures above 273 K, a vertical signal expansion shows (see Figure S3, SI) that it is already present at 248 K. Upon heating, the intensity of the coalesced signal grows and dominates above 303 K. A quantitative analysis of these features will be given later.

Variable Temperature $^{1}H-^{15}N$ CPMAS HETCOR and ^{1}H MAS NMR Spectroscopy of Cell-Im-^{15}N. The question now arises what type of hydrogen bonds dominate the interactions between cellulose, imidazole, and water. To solve this puzzle, we have performed frequency switched Lee−Goldburg $^{1}H-^{15}N$ HETCOR experiments.[42,53,54,59,61−63] In these experiments, ^{1}H homonuclear interactions are decoupled during the evolution time t_1 to prevent ^{1}H spin diffusion and enhance the spectral resolution of the ^{1}H dimension.

Figures 2 and 3 depict the two-dimensional $^{1}H-^{15}N$ HETCOR spectra of Im-^{15}N and of Cell-Im-^{15}N recorded at

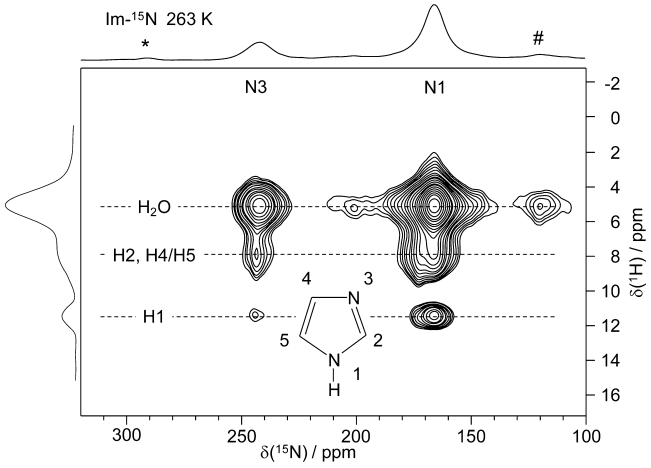

Figure 2. 2D $^{1}H-^{15}N$ HETCOR spectrum recorded at 14.1 T of Im-^{15}N at 263 K.

263 and 243 K, respectively. Figure 4a,b shows the one-dimensional projections into the ^{1}H dimension retrieved from the 2D spectra. We note that the signals shown arise all from $^{1}H-^{15}N$ cross peaks. ^{1}H nuclei that are far away from ^{15}N do not appear. We estimate that the margin of error of the chemical shifts is about 1 ppm because of the frequency scaling problems in $^{1}H-^{15}N$ HETCOR experiments, as addressed in the Experimental Section. In addition, a ^{1}H MAS spectrum obtained at room temperature is included (Figure 4c), where all protons of the sample contribute to the spectrum.

Let us first analyze the 1D projection of the 263 K $^{1}H-^{15}N$ HETCOR spectrum of Im-^{15}N into the ^{1}H dimension, depicted

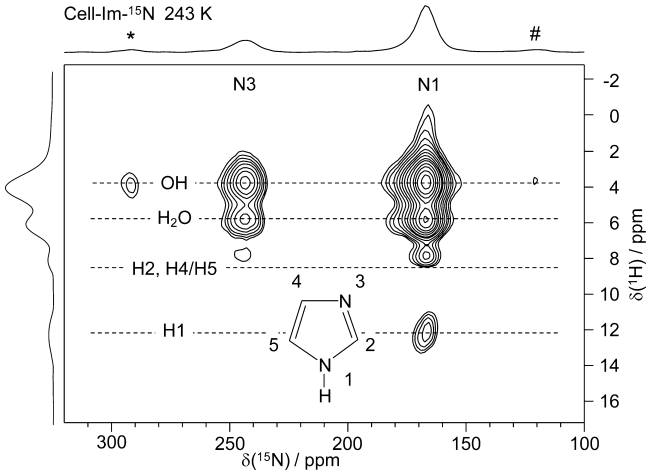

Figure 3. 2D $^{1}H-^{15}N$ HETCOR spectrum recorded at 14.1 T of Cell-Im-^{15}N at 243 K. For additional spectra at higher temperatures, see the SI.

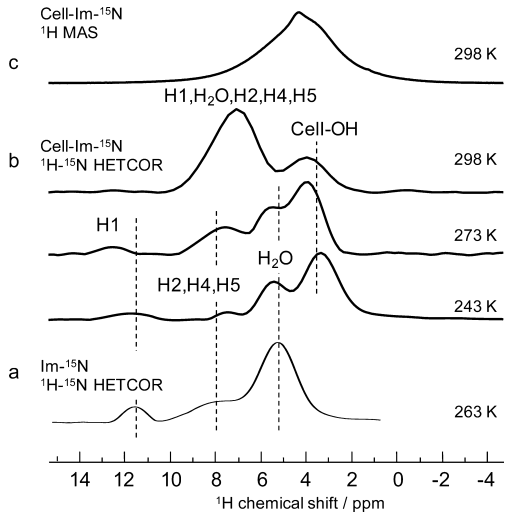

Figure 4. (a) 1D ^{1}H spectrum of Im-^{15}N retrieved from Figure 2. (b) ^{1}H spectra of Cell-Im-^{15}N retrieved from Figure 3 and other 2D HETCOR spectra depicted in the SI. (c) ^{1}H one pulse MAS spectrum of Cell-Im-^{15}N recorded at 14.1 T and 298 K using a spinning rate of 60 kHz.

in Figure 4a. The assignment is straightforward, that is, the imidazole NH protons (H1), which exchange only slowly with water, resonate around 12 ppm, as expected.[41] The aromatic hydrogens appear between 6 and 9 ppm, and a strong water signal is observed around 5 ppm. In the corresponding spectrum of Cell-Im-^{15}N (Figure 4b), an additional high-field peak around 3−4 ppm is observed, arising almost entirely from protons located near to the imidazole nitrogens. Therefore, we assign this signal to OH-groups of cellulose. Up to 273 K, within the margin of error, only minor changes occur, whereas at room temperature a very broad peak around 7 ppm is observed, corresponding to a superposition of aromatic imidazole protons and to fast exchanging NH-protons of imidazole and OH-groups of water and cellulose. Slowly exchanging cellulose−OH groups give rise to the peak around 4 ppm.

On the other hand, in the ^{1}H MAS spectrum at room temperature (Figure 4c), only one broad peak can be resolved

DOI: 10.1021/acs.jpcc.6b07049
J. Phys. Chem. C 2016, 120, 19574−19585

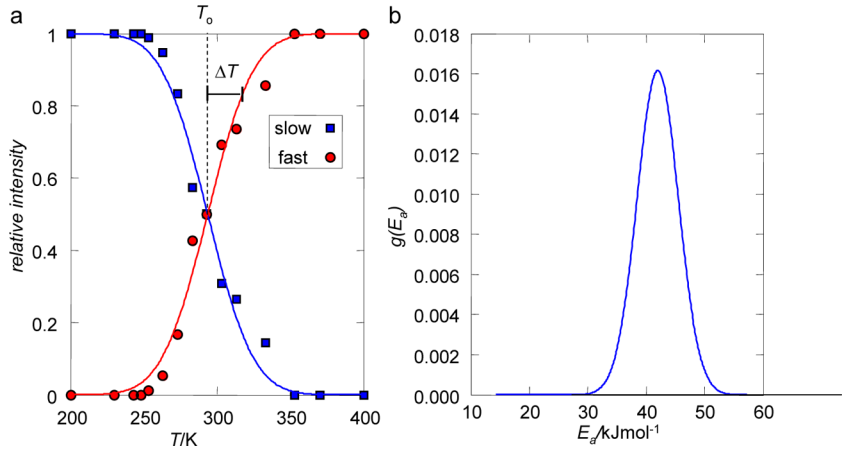

Figure 5. (a) Fractions of the slow and fast exchanging amino and imino nitrogens of Cell-Im-^{15}N derived from the spectra depicted in Figure 1 and their simulation according to eq 5 in ref 80. (b) Activation energy distribution of the proton tautomerism of imidazole in cellulose.

around 4 ppm. We assign this signal to aliphatic cellulose protons.

After having performed the ^{1}H signal we are now able to retrieve the information on the 2D HETCOR spectra. The main information concerns imidazole in Cell-Im-^{15}N (Figure 4b). Not only imidazole N1-water and N3-water contacts are observed, but also contacts of both nitrogens with cellulose−OH groups. These contacts can refer both to dipolar couplings within NHO and OHN hydrogen bonds, as well as to couplings to further distant protons. These results are consistent only with intimately mixed imidazole-cellulose domains, where imidazole is hydrogen bonded both to cellulose−OH groups and to water molecules.

In Figure S4 of the SI are depicted 2D ^{1}H−^{15}N HETCOR spectra recorded at 273 and 298 K. Broad peaks are observed that are difficult to resolve. The spectra indicate again that the tautomerism of imidazole is coupled to proton exchange with water and cellulose OH groups.

Discussion. In this section we will discuss the implications of our studies of wet imidazole and of imidazole/cellulose mixtures (Cell-Im) for the structure and function of these systems.

Quantitative Analysis of Observed Variable-Temperature ^{15}N Solid State NMR Spectra. The question arises of which information we can obtain on the tautomerism of imidazole in cellulose by discussion of the variable temperature ^{15}N CPMAS spectra depicted in Figure 1. In contrast to the usual broadening and coalescence of amino and imino nitrogen signals[64−70] from which rate constants of proton tautomerizations can be derived, we observe here between 263 and 353 K a superposition of two phases, one characterized by slow tautomerizations exhibiting separate amino (N1) and imino (N3) signals containing rotational side bands, and another liquid-type sharp coalesced average N1/N3 signal without sidebands. That means that the tautomerism is coupled to fast molecular reorientations. When temperature is increased, the fraction of the slowly exchanging rigid molecules decreases, and the fraction of the rapidly exchanging and reorientating molecules increases, as depicted in Figure 5a.

These findings indicate a distribution of imidazole tautomerization rate constants arising from a local structural heterogeneity. Whereas related phenomena have been observed before in cases of molecular reorientations in disordered solids[71] or melting processes,[72] only some cases of distributions of tautomerizations have been reported up to date.[73−75] Thus, to our knowledge, no similar case of a heterogeneous solid state imidazole or histidine tautomerism has been reported up to date.

A simple way to determine the distribution of activation energies for the tautomerism is the two-phase model, initially proposed by Roessler et al.[76] in the context of glass-dynamics and later applied to other disordered systems.[77,78] The solid Gaussian type lines in Figure 5a were calculated according to this model using a laboratory written MATLAB program.[72] The main line parameters are the center-temperature T_0 = 293.6 K and the temperature width ΔT = 24.7 K. The former describes the temperature where the two-phase fractions are 0.5. The latter characterizes the temperature interval in which the transition from slow to fast exchange spectra takes place. Using these parameters, the Gaussian activation energy distribution can be estimated as illustrated in Figure 5b. The main activation energy is E_a = 42 kJ/mol, and the corresponding standard deviation of the distribution is ΔE_a = 3.5 kJ/mol, corresponding to a full width at half-height of the Gaussian curve of 8.2 kJ/mol.

Assuming a pre-exponential factor on the order of 10^{-12} s^{-1}, an Arrhenius ansatz calculates typical exchange rate constants in the range of 10^{4}−10^{5} s^{-1} at 293 K. This value range is much smaller as compared to the value of 10^{7} s^{-1} at 298 K estimated for the tautomerization of 4-methyl-imidazole dissolved in the wet polar organic solvent mixture CDF_3/CDF_2Cl.[41] We will discuss these findings later in more detail.

Hydrogen Bonding and Proton Exchange of Imidazole with Water or with Cellulose? In order to answer this question, we performed the two-dimensional ^{1}H−^{15}N NMR experiments on ^{15}N-labeled imidazole (Im-^{15}N) and imidazole embedded in cellulose (Cell-Im-^{15}N), depicted in Figures 2 and 3. The variable-temperature ^{1}H projections assembled in Figure 4a,b stem only from dipolar coupled ^{1}H nuclei located nearby the imidazole nitrogen atoms. For comparison, Figure 4c depicts the room-temperature ^{1}H MAS spectrum to which all protons of the sample contribute. In spite of the scaling of the chemical shift axis leading to chemical shift errors up to 1 ppm, in the Cell-Im-^{15}N spectra below 273 K peaks appear for **N1**-H of imidazole between 11 and 12 ppm, for water between 5 and 6 ppm and for cellulose−OH between 3 and 4 ppm. At 293 K, these peaks have coalesced to a great peak. These findings indicate that (*i*) imidazole forms OHN bonds, both to water

DOI: 10.1021/acs.jpcc.6b07049
J. Phys. Chem. C 2016, 120, 19574−19585

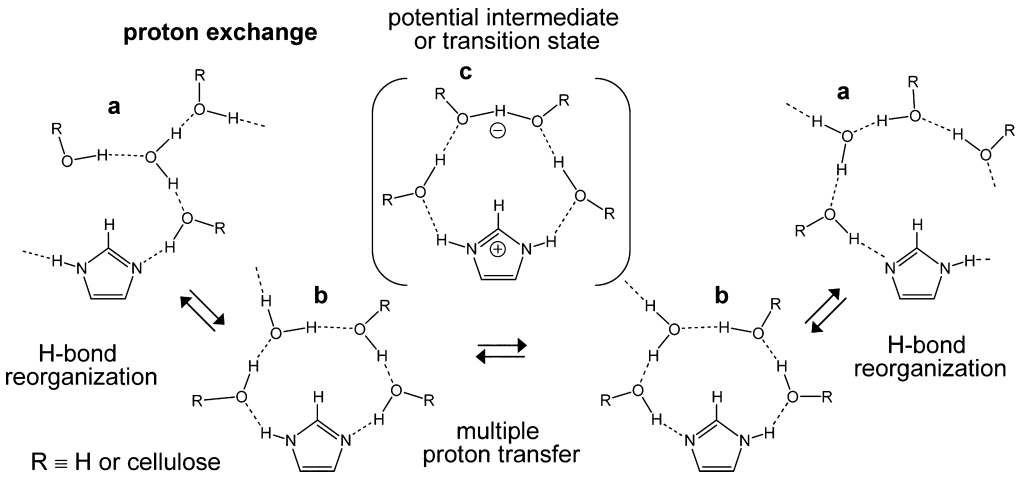

Figure 6. Proton exchange of imidazole with water in wet aprotic environments according to ref 41. No contribution to proton conductivity.

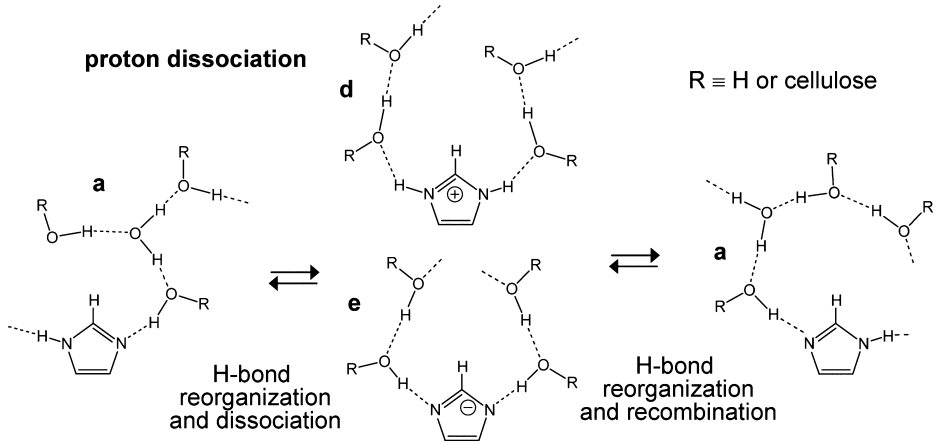

Figure 7. Proton exchange of imidazole with water via dissociation in polar environments. Contributes to proton conductivity.

and to cellulose−OH groups and that (*ii*) the tautomerism of imidazole is coupled to proton exchange with water and cellulose−OH groups.

As at 293 K, there is still a substantial part of the imidazole molecules exhibiting a slow tautomerization it is not surprising that there are residual N1−H and OH signals that are still in slow exchange.

Mechanism of Proton Tautomerism and Proton Exchange of Imidazole with Water and Cellulose OH-Groups: Implications for Proton Conductivity. The observation that the imidazole tautomerism is coupled to proton exchange with water and cellulose OH-groups agrees well with a similar previous finding for 4-methyl-imidazole dissolved in wet CDF_3/CDF_2Cl.[41] In that work, coalescence of the amino and imino nitrogen signals was also coupled to a coalescence of the imidazole NH and water proton signals. From these findings, the mechanism depicted in Figure 6 was derived.

Imidazole forms mainly linear hydrogen bonded complexes with water clusters of various sizes and structures. Structure **a** represents only one possibility. Hydrogen bond reorganization is fast and can lead sometimes to the formation of cyclic intermediates **b**. In these intermediates proton exchange can take place, consisting of multiple OHN and OHO proton transfers. In Figure 6 five protons are supposed to move, but there will be other configurations where a smaller or a larger number of proton will be transferred. As has been discussed previously,[79] proton transfer is coupled to hydrogen bond compression. As at one time only up to 3 hydrogen bonds can be compressed, leading to a concerted multiple proton transfer, zwitterionic intermediates or transition states such as structure **c** will most probably be involved in the case of clusters of imidazole with water and other proton donors such as cellulose−OH groups. The most important feature is that it requires a high molecular mobility of OH groups and of the imidazole molecules. That was confirmed by the observation in Figure 1 that the liquid-type coalesced N1/N3 signal of imidazole does not exhibit a rotational sideband pattern.

We note that the mechanism of Figure 6 does not contribute to the proton conductivity observed by some of us.[21] That is not surprising as the latter exhibits an energy of activation of 103 kJ mol^{-1}, whereas we observe here an average energy of 42 kJ mol^{-1}. The question now arises, what is the reason for this difference?

In Figure 7 we have depicted as an alternative a dissociation mechanism that involves also initial hydrogen bond reorganization but followed by dissociation into a "free" solvated imidazolium cation **d** and a "free" solvated imidazolate anion **e**. Subsequently, protons are transferred rapidly between water, cellulose−OH and imidazole species. As has been shown before, the energy of activation of this mechanism is increased by half of the enthalpy of dissociation as the number of proton carriers increases with temperature.[80] That enthalpy will

DOI: 10.1021/acs.jpcc.6b07049
J. Phys. Chem. C 2016, 120, 19574−19585

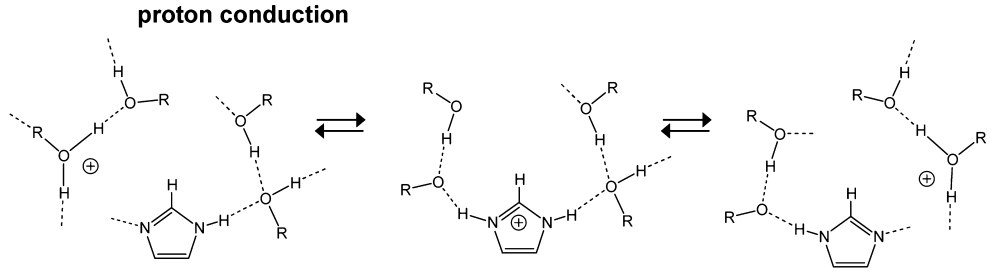

Figure 8. Acid-induced proton conductivity of imidazole in polar environments.

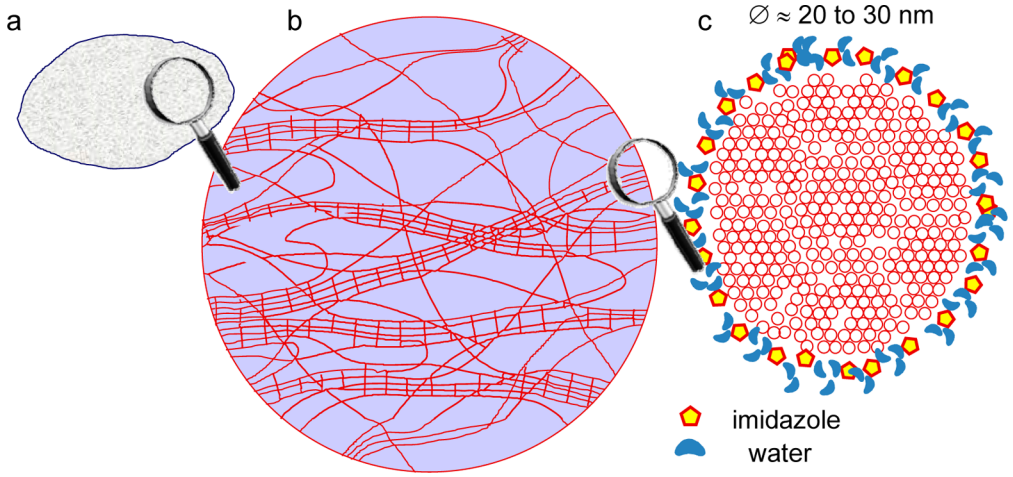

Figure 9. Structure of Cell-Im. (a) Schematic view of a single cellulose grain (macrofibril). (b) Cellulose model according to Hearle[81] showing schematic assemblies of polysaccharide chains with disordered chains in amorphous regions and parallel chains in microcrystalline regions (microfibrils). (c) Cross section of a microfibril of Cell-Im into which imidazole and water cannot penetrate. Note: As added imidazole forms hydrogen bonds to cellulose−OH groups and to residual water molecules it must be located on the microfibril surfaces. Water-free imidazole clusters in pores would lead to N−H···N hydrogen bonds, which are not observed.

depend strongly on the local polarity and water content. In contrast to the proton exchange mechanism, the dissociation mechanism will contribute to the proton conductivity of cellulose−imidazole composites. That might explain why the energy of activation of conductivity is much larger than of the tautomerism and proton exchange.

Finally, we wish to note that the addition of acids to the cellulose surfaces might increase the proton transfer rates and hence of the proton conductivity by the formation of imidazolium, as illustrated in Figure 8. That will be the case when Cell-Im is embedded in a fuel cell as proton conducting membrane, where H^+ is created at the anode by oxidation of dihydrogen and where the electron created is transferred to the cathode via an electrical wire.

We note that processes discussed in this section, namely, the tautomerism of imidazole in Cell-Im coupled to proton exchange, the dissociation mechanism as well as the acid-induced proton conductivity all are enabled by the local mobility in the pores of cellulose, created by residual water molecules.

Some Remarks about the Structure of Cell-Im. Some important features of microcrystalline cellulose into which the imidazole was loaded are illustrated in Figure 9. SEM experiments of Cell-Im show that it consists of grains, also called "macrofibrils". A partial SEM picture showing some grains is depicted in Figure 9a. The size of the grains is of the order of 20 μm. According to Hearle,[81] these macrofibrils contain both amorphous as well as crystalline regions, as illustrated schematically in Figure 9b. The crystalline regions consist of parallel polysaccharide chains, where only a small number of chains are shown for clarity. According to Zhao et al.,[33] water and acids can penetrate into macrofibrils and lead to the hydrolysis of the chains until only neat crystalline nanofibrils remain. The latter exhibit diameters of the order of 20−30 nm, as illustrated in Figure 9c.

It has been argued by some of us[21] that imidazole will not enter crystalline cellulose regions but will be bound to polymer chains at their surfaces. Here, by NMR we confirm this argument. As crystalline cellulose regions are rigid, also imidazole molecules inside such a region will not reorientate rapidly as found here and discussed above. Therefore, rapidly reorientating imidazole is only found together with water as a lubricant close to the inner cellulose surfaces or in local pores.

A rough estimate of the size of the fibrils of Cell-Im into which imidazole and water cannot penetrate is obtained from the finding of about 1 imidazole molecule per 5 anhydroglucose repeat units. Let us assume that one imidazole is bound to each repeat unit in the surface. Then, the ratio of the number of surface chains to all chains is given by the surface section area divided by the total chain section, that is

$$R = \frac{\text{total chain section area}}{\text{surface shell area}} = \frac{\pi r^2}{\pi r^2 - \pi(r-l)^2} = 5$$

where $2r$ represents the fibril diameter and l the chain diameter. Assuming that l = 1 nm it follows that $2r$ = 20 nm, which is in excellent agreement with the findings of Zhao et al. for

DOI: 10.1021/acs.jpcc.6b07049
J. Phys. Chem. C 2016, 120, 19574−19585

microfibrils.[33] In other words, one crystalline microfibril will contain about 300 polymer chains.

We note that if one assumes that the nonwater-penetrable crystalline fibrils are much larger, their surface area decreases and only a smaller quantity of imidazole molecules can be bound to the polysaccharide chains. The remaining imidazole molecules must then be located in pores where they could assemble and form NHN-hydrogen bonds, in contrast to our findings of only OHN hydrogen bonds from and to imidazole.

B. DNP Enhanced ^{13}C and ^{15}N Solid State NMR Spectroscopy of Cell-Im-TOT and Im-TOT at 105 K. *Results.* ^{15}N-solid state NMR is the most powerful approach to monitor the hydration state of heterocycles. The main obstacle in its application is the low sensitivity at ^{15}N natural abundance. While ^{15}N-enriched imidazole is commercially available, this is not the case for most other heterocycles. For this reason, we wanted to evaluate whether DNP enhancement is a possible strategy to widen the range of guest heterocycles or whether the addition of the DNP radical solution changes the structure of the system. To answer these questions, we studied the DNP-enhanced ^{13}C and ^{15}N-CP-MAS spectra of Cell-Im-TOT and Im-TOT.

Figure 10a shows the DNP enhanced ^{13}C CPMAS spectra of the "pure" imidazole sample Im-TOT obtained with microwave

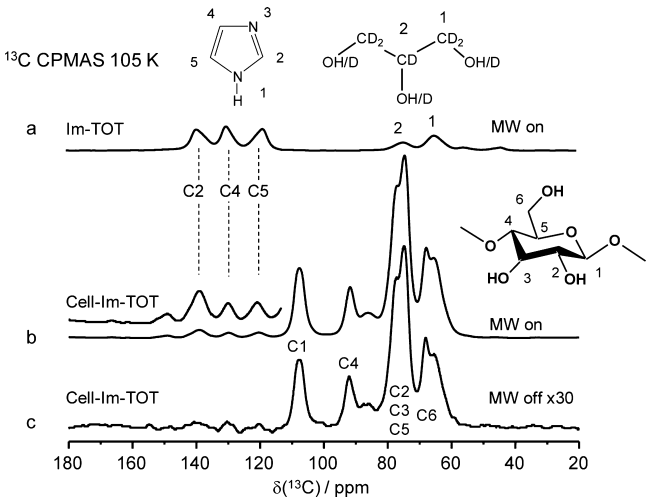

Figure 10. ^{13}C CP MAS NMR spectra of Im-TOT (a) and Cell-Im-TOT with (b) and without (c) microwave irradiation.

irradiation. The imidazole carbon signals are observed at low field; their assignment is straightforward and consist with the pure imidazole ^{13}C CPMAS (Figure S2, SI). At high field, two small signals are observed in the aliphatic region, which stem from glycerol in the added TOTAPOL solution. By signal integration a molar ratio of about 2:1 is obtained, but signal intensity ratios are altered both by DNP and by CP and cannot be directly used to determine the sample composition.

Furthermore, the signals of glycerol are most probably overlaid with signals of cellulose (C6), which are also obtainable in the region of 60−70 ppm (see for example ref 82).

The imidazole carbon signals also appear in the DNP enhanced spectrum of Cell-Im-TOT depicted in Figure 10b, indicating that imidazole is contained in the sample. In addition, the expected cellulose signals appear at high field. Their assignment to the cellulose ring carbons was performed according to Kono et al.[83] As illustrated in Figure 10, the signal at the highest field is composed of two parts: we assign the low-field part to C6 and the high-field component to the methylene groups of added glycerol.

The signal enhancement by DNP is demonstrated in Figure 10c. Without microwave irradiation, the signal intensities are about 30 times smaller than with irradiation.

In summary, in spite of the TOTAPOL radical added, the carbon signals of imidazole, cellulose and glycerol carbons appear at the expected places and are not altered within the margins of error by the radical addition.

In order to illustrate the nature of the imidazole nitrogens in the Cell-Im material, as well as to study the influence of the DNP radical matrix on the hydrogen bonds in this sample, ^{15}N CPMAS as well as ^{15}N CPMAS DNP experiments at 105 K were performed that are depicted in Figure 11. While the

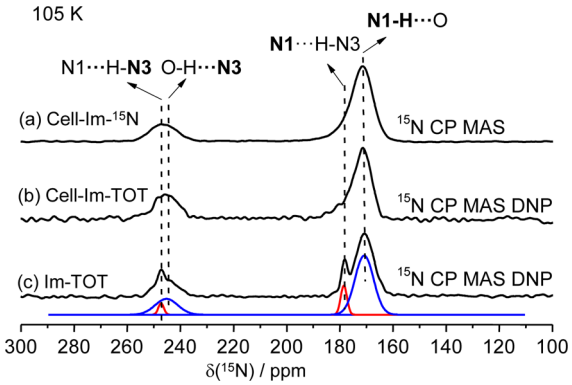

Figure 11. ^{15}N CPMAS spectrum of (a) ^{15}N enriched imidazole embedded in cellulose (Cell-Im-^{15}N) without radical matrix, (b) non-^{15}N enriched Cell-Im-TOT using DNP enhancement, and (c) non-^{15}N enriched Im-TOT using DNP enhancement. The spectra were measured at 9.4 T and 105 K at a spinning speed of 7.5 kHz. Note: Spinning sidebands that are outside of the displayed spectral range.

reference sample Cell-Im-^{15}N (Figure 11a) contained ^{15}N enriched imidazole without added radical matrix, the samples Cell-Im-TOT (Figure 11b) and Im-TOT (Figure 11c) contained ^{15}N at natural abundance and were impregnated with TOTAPOL solution.

All spectra exhibit the characteristic low-field imino (=N-) and the high-field amino (>NH) signals of imidazole. The amino signal is stronger than the imino signal because of different CP dynamics. All signals are broad, their line width is about 10 ppm, a feature which will be discussed later. No essential difference between the spectra of Figure 11a and 11b are detected; therefore, the TOTAPOL radical does not affect the chemical shifts of the DNP enhanced signals.

The spectrum of Im-TOT exhibits the same broad signals as the Cell-Im samples, but in addition two sharp slightly low-field shifted imino and amino signals are observed. These signals are typical for crystalline imidazole exhibiting NHN hydrogen bonds.[41] The high-field shifts of the broad amino and imino signals are typical for the formation of N−H···O and N···H−O as a comparison with ^{15}N chemical shift data of hydrogen bonded imidazole complexes reveals. We assign, therefore, the broad lines to imidazole embedded in a matrix of cellulose and water OH-groups.

Discussion. Comparison of Results from Low-Temperature CPMAS and CPMAS DNP NMR. When Cell-Im or pure

DOI: 10.1021/acs.jpcc.6b07049
J. Phys. Chem. C 2016, 120, 19574−19585

imidazole samples are doped with a small quantity of a TOTAPOL radical solution and irradiated with microwaves, dynamic nuclear polarization (DNP) results by which ^{1}H spin polarization is created which is then transferred to ^{13}C or ^{15}N by cross-polarization. That leads to a considerable ^{13}C signal enhancement, as depicted in Figure 10. Interestingly, besides the different signal intensities, the ^{13}C CPMAS spectra with and without microwave irradiation are the same. These observations refer to the following.

As has been established before,[84−87] the nuclei whose NMR signals are enhanced by DNP are located at a certain distance from the paramagnetic centers. Thus, the latter do not perturb the local structure and the NMR parameters of the polarized nuclei observed. Nuclei which are located closer to the paramagnetic centers are not observed because of distance-dependent electron−nucleus spin interactions. In addition, the polarization does not remain near the cellulose surfaces but is transferred into the interior of the cellulose fibers by ^{1}H spin diffusion typical for organic solids.[88] Therefore, results from CPMAS DNP measurements are directly comparable to those obtained by CPMAS alone.

The circumstance that nuclei which are located sufficiently far from the TOTAPOL radicals can experience signal enhancements without perturbation of local structures and hence of NMR parameters is demonstrated also by the following findings. The ^{15}N CPMAS spectrum of ^{15}N enriched Cell-Im-^{15}N (Figure 11a) and the ^{15}N CPMAS DNP spectrum of nonenriched Cell-Im-TOT but doped with TOTAPOL (Figure 11b) are essentially the same, both with respect to chemical shifts and to line widths.

OHN and NHO Hydrogen Bond Formation of Imidazole in the Wet Pure Solid and in Cellulose Detected by ^{15}N NMR. The ^{15}N chemical shifts of imidazole and its derivatives have been correlated recently with the corresponding ^{1}H chemical shifts and hence with the imidazole hydrogen bond and protonation state.[41] This correlation allows us now to characterize the hydrogen bonded state of imidazole in the different environments studied.

Particularly interesting are the ^{15}N CPMAS DNP spectra of wet pure imidazole doped with TOTAPOL (Im-TOT) recorded at 105 K (Figure 11c). The two small sharp imino and amino signals stem from a small quantity of pure polycrystalline imidazole forming only N1−H···N3 hydrogen bonds. A substantial part of imidazole is, however, embedded in a solid glycerol-d_8/D_2O/H_2O matrix forming N1−H···O hydrogen bonds, which leads to small high-field shifts and a broadening of the signals.

According to the imidazole hydrogen bond correlations,[41] the observed high-field shift of 7 ppm of the imidazole amino nitrogen (N1) indicates a shortening of the N−H distance in the N1−H···O hydrogen bond of about 0.02 Å. This is in agreement with a weakening of this bond. By contrast, the high-field shift of 3 ppm of the imidazole imino nitrogen (N3) indicates a shortening of the N···H distance of about 0.06 Å. The longer the hydrogen bonded water chain, the larger is the shortening of the hydrogen bond, that is, the high-field shift as found previously for pyridine embedded in ice.[41] As the matrix is inhomogeneous, the broadening of the signals indicates a distribution of hydrogen bond geometries. We note that it is well-known that on average O−H···N hydrogen bonds are stronger than N−H···N hydrogen bonds, and N−H···O hydrogen bonds are weaker.[75]

When imidazole is embedded in cellulose, only N1−H···O and O−H···N3 hydrogen bonds are observed. They are formed with water and with cellulose OH and O groups. The spectra of Cell-Im-^{15}N and of Cell-Im-TOT agree very well. Again, the hydrogen bond geometries observed by both methods are the same within the margin of error.

The formation of OHN-hydrogen bonds has been postulated previously by some of us,[21] based on a comparison of IR spectra of pure cellulose and of imidazole-doped cellulose. The present ^{15}N NMR results confirm this conclusion entirely.

CONCLUSIONS

(i) A ^{15}N chemical shift analysis and two-dimensional $^{1}H-^{15}N$ HETCOR experiments reveal that imidazole in Cell-Im only forms N−H···O and O−H···N hydrogen bonds, both to residual water molecules as well as to cellulose−OH groups. Thus, imidazole is located mainly on the polysaccharide surfaces.

(ii) Molecular reorientation of imidazole assisted by the presence of residual water molecules activates the imidazole tautomerism in Cell-Im. Temperature-dependent ^{15}N and $^{1}H-^{15}N$ HETCOR NMR spectra reveal that the tautomerism does not take place between imidazole molecules alone, but that it is coupled to proton exchange both with water and cellulose−OH molecules. Several water or OH-groups are necessary for the proton exchange to occur. So-called "two-phase" ^{15}N spectra are observed, indicating a temperature-dependent broad distribution of rapidly and slowly exchanging imidazole water clusters. An analysis of the ratio of both signal types indicates a main activation energy of about 42 kJ mol^{-1}. This value is much larger than the one found previously[41] for 4-methyl-imidazole in wet organic solvent. Thus, imidazole-water forms a fluid phase within Cell-Im, exhibiting a molecular mobility between an organic solid and an organic liquid.

(iii) The proton exchange of imidazole with water observed in Cell-Im does not contribute to the proton conductivity observed by some of us previously.[21] However, the structural features, in particular, the local mobility of imidazole assisted by residual water and cellulose−OH groups that activates the observed proton exchange, are also a prerequisite of the proton conductivity.

A mechanism where imidazole dissociates into imidazolium and imidazolate may be present as a minor pathway of proton exchange. This mechanism will exhibit a much larger activation energy as it is increased by half of the dissociation enthalpy. That mechanism, however, may be responsible for the proton conductivity of Cell-Im. Also, added acid will enhance the conductivity, but no acid presence was observed in the samples studied here, as it would lead to high-field shifts of the coalesced imidazole ^{15}N signal.

(iv) The cellulose fibers of Cell-Im consist of a network of rigid crystalline fibrils containing a fluid of an imidazole/water mixture. Thus, the cellulose network provides the mechanical stability of a solid material, whereas the fluid inside is responsible for the molecular motions, proton exchange, and proton conductivity.

(v) The comparison of low-temperature standard and DNP enhanced ^{13}C and ^{15}N CPMAS NMR spectra of imidazole-doped cellulose (Cell-Im) shows that DNP

DOI: 10.1021/acs.jpcc.6b07049
J. Phys. Chem. C 2016, 120, 19574−19585

enhancement does not influence the structure of the systems and is thus able to reveal information about the chemical and hydrogen bond structure of heterocycles with natural abundance ^{15}N.

■ ASSOCIATED CONTENT

Supporting Information

The Supporting Information is available free of charge on the ACS Publications website at DOI: 10.1021/acs.jpcc.6b07049.

Experimental and characterization details, including NMR spectroscopic data, SEM, and experimental details (PDF).

■ AUTHOR INFORMATION

Corresponding Authors

*Phone: +49 6151/16-21116. E-mail: gerd.buntkowsky@chemie.tu-darmstadt.de.

*Phone: +49 6151/16-21120. E-mail: gutmann@chemie.tu-darmstadt.de.

*Phone: +48 61 8695 226. E-mail: jtg@ifmpan.poznan.pl.

Author Contributions

†These authors contribute equally to this work (L.Z., I.S., and H.-H.L.).

Notes

The authors declare no competing financial interest.

■ ACKNOWLEDGMENTS

This work has been supported by the Deutsche Forschungsgemeinschaft (DFG) under Contract Bu-911-20-1. G.B. gratefully acknowledges financial support by the state of Hessia, LOEWE iNAPO. This work was supported by the European Social Fund within the project development of common Ph.D. studies in nanotechnology-electronics and photovoltaics in the Institute of Molecular Physics of Polish Academy of Sciences and at the Faculty of Physics at Adam Mickiewicz University in Poznan (POKL.04.03.00-00-015/12).

■ REFERENCES

(1) Minh, N. Q. Ceramic Fuel Cells. *J. Am. Ceram. Soc.* **1993**, *76*, 563−588.

(2) Tarascon, J. M.; Armand, M. Issues and Challenges facing Rechargeable Lithium Batteries. *Nature* **2001**, *414*, 359−367.

(3) Kreuer, K. D. On the development of Proton Conducting Materials for technological applications. *Solid State Ionics* **1997**, *97*, 1−15.

(4) Padhi, A. K.; Nanjundaswamy, K.; Goodenough, J. Phospho-olivines as Positive-Electrode Materials for Rechargeable Lithium Batteries. *J. Electrochem. Soc.* **1997**, *144*, 1188−1194.

(5) Carrette, L.; Friedrich, K.; Stimming, U. Fuel Cells−Fundamentals and Applications. *Fuel Cells* **2001**, *1*, 5−39.

(6) Gasteiger, H. A.; Kocha, S. S.; Sompalli, B.; Wagner, F. T. Activity Benchmarks and Requirements for Pt, Pt-alloy, and non-Pt Oxygen Reduction Catalysts for PEMFCs. *Appl. Catal., B* **2005**, *56*, 9−35.

(7) Li, Q.; He, R.; Gao, J.-A.; Jensen, J. O.; Bjerrum, N. J. The CO poisoning Effect in PEMFCs operational at Temperatures up to 200 C. *J. Electrochem. Soc.* **2003**, *150*, A1599−A1605.

(8) Song, S.; Tsiakaras, P. Recent Progress in Direct Ethanol Proton Exchange Membrane Fuel Cells (DE-PEMFCs). *Appl. Catal., B* **2006**, *63*, 187−193.

(9) Xing, B.; Savadogo, O. Hydrogen/Oxygen Polymer Electrolyte Membrane Fuel Cells (PEMFCs) based on Alkaline-doped Polybenzimidazole (PBI). *Electrochem. Commun.* **2000**, *2*, 697−702.

(10) Curtin, D. E.; Lousenberg, R. D.; Henry, T. J.; Tangeman, P. C.; Tisack, M. E. Advanced Materials for improved PEMFC Performance and Life. *J. Power Sources* **2004**, *131*, 41−48.

(11) Mauritz, K. A.; Moore, R. B. State of Understanding of Nafion. *Chem. Rev.* **2004**, *104*, 4535−4586.

(12) Gierke, T.; Munn, G.; Wilson, F. The Morphology in Nafion Perfluorinated Membrane Products, as Determined by Wide-and Small-Angle X-ray Studies. *J. Polym. Sci., Polym. Phys. Ed.* **1981**, *19*, 1687−1704.

(13) Kreuer, K. D. On Solids with Liquidlike Properties and the Challenge To Develop New Proton-Conducting Separator Materials for Intermediate-Temperature Fuel Cells. *ChemPhysChem* **2002**, *3*, 771−775.

(14) Kreuer, K. On the Development of Proton Conducting Polymer Membranes for Hydrogen and Methanol Fuel Cells. *J. Membr. Sci.* **2001**, *185*, 29−39.

(15) Asensio, J. A.; Gomez-Romero, P. Recent Developments on Proton Conducting Poly (2, 5-benzimidazole) (ABPBI) Membranes for High Temperature Polymer Electrolyte Membrane Fuel Cells. *Fuel Cells* **2005**, *5*, 336−343.

(16) Beyazyildirim, S.; Kreuer, K. D.; Schuster, M.; Bhattacharyya, A. J.; Maier, J. Heterogeneous Doping of a Weak Covalent Electrolyte: Proton Conductivity Enhancement of Imidazole by Admixture of Oxide Particles. *Adv. Mater.* **2008**, *20*, 1274−1278.

(17) Kreuer, K.; Fuchs, A.; Ise, M.; Spaeth, M.; Maier, J. Imidazole and Pyrazole-based Proton Conducting Polymers and Liquids. *Electrochim. Acta* **1998**, *43*, 1281−1288.

(18) Kalia, S.; Dufresne, A.; Cherian, B. M.; Kaith, B.; Avérous, L.; Njuguna, J.; Nassiopoulos, E. Cellulose-based Bio- and Nanocomposites: a Review. *Int. J. Polym. Sci.* **2011**, *2011*, 1−35.

(19) Yamada, M.; Honma, I. A Biopolymer Composite Material as an Anhydrous Proton-Conducting Membrane. *Angew. Chem.* **2004**, *116*, 3774−3777.

(20) Yamada, M.; Honma, I. Alginic Acid−Imidazole Composite Material as Anhydrous Proton Conducting Membrane. *Polymer* **2004**, *45*, 8349−8354.

(21) Smolarkiewicz, I.; Rachocki, A.; Pogorzelec-Glasser, K.; Pankiewicz, R.; Ławniczak, P.; Łapiński, A.; Jarek, M.; Tritt-Goc, J. Proton-conducting Microcrystalline Cellulose Doped with Imidazole. Thermal and Electrical Properties. *Electrochim. Acta* **2015**, *155*, 38−44.

(22) Samsudin, A.; Lai, H.; Isa, M. Biopolymer Materials based Carboxymethyl Cellulose as a Proton Conducting Biopolymer Electrolyte for Application in Rechargeable Proton Battery. *Electrochim. Acta* **2014**, *129*, 1−13.

(23) Zhou, T.; Chen, D.; Jiu, J.; Nge, T.; Sugahara, T.; Nagao, S.; Koga, H.; Nogi, M.; Suganuma, K.; Wang, X. Electrically Conductive Bacterial Cellulose Composite Membranes produced by the Incorporation of Graphite Nanoplatelets in pristine Bacterial Cellulose Membranes. *eXPRESS Polym. Lett.* **2013**, *7*, 756−766.

(24) Kreuer, K. D.; Fuchs, A.; Ise, M.; Spaeth, M.; Maier, J. Imidazole and Pyrazole-based Proton Conducting Polymers and Liquids. *Electrochim. Acta* **1998**, *43*, 1281−1288.

(25) Schmidt-Rohr, K.; Chen, Q. Parallel cylindrical Water Nanochannels in Nafion Fuel-Cell Membranes. *Nat. Mater.* **2008**, *7*, 75−83.

(26) Goward, G. R.; Saalwächter, K.; Fischbach, I.; Spiess, H. W. Reorientation Phenomena in Imidazolium Methyl Sulfonate as probed by advanced Solid-State NMR. *Solid State Nucl. Magn. Reson.* **2003**, *24*, 150−162.

(27) Song, X.-j.; McDermott, A. E. Proton transfer Dynamics and N—H bond Lengthening in N—H···N model systems: a solid-state NMR study. *Magn. Reson. Chem.* **2001**, *39*, S37−S43.

(28) Fisher, S. Z.; Kovalevsky, A. Y.; Domsic, J. F.; Mustyakimov, M.; McKenna, R.; Silverman, D. N.; Langan, P. A. Neutron Structure of Human Carbonic Anhydrase II: Implications for Proton Transfer. *Biochemistry* **2010**, *49*, 415−421.

(29) Bureekaew, S.; Horike, S.; Higuchi, M.; Mizuno, M.; Kawamura, T.; Tanaka, D.; Yanai, N.; Kitagawa, S. One-dimensional Imidazole

Aggregate in Aluminium Porous Coordination Polymers with high Proton Conductivity. *Nat. Mater.* **2009**, *8*, 831−836.
(30) Dupuis, A.-C. Proton Exchange Membranes for Fuel Cells operated at medium Temperatures: Materials and experimental Techniques. *Prog. Mater. Sci.* **2011**, *56*, 289−327.
(31) Hu, F.; Luo, W.; Hong, M. Mechanisms of Proton Conduction and Gating in Influenza M2 Proton Channels from Solid-State NMR. *Science* **2010**, *330*, 505−508.
(32) Nishiyama, Y.; Langan, P.; Chanzy, H. Crystal Structure and Hydrogen-bonding System in Cellulose Iβ from Synchrotron X-ray and Neutron Fiber Diffraction. *J. Am. Chem. Soc.* **2002**, *124*, 9074−9082.
(33) Zhao, H.; Kwak, J. H.; Zhang, Z. C.; Brown, H. M.; Arey, B. W.; Holladay, J. E. Studying Cellulose Fiber Structure by SEM, XRD, NMR and Acid Hydrolysis. *Carbohydr. Polym.* **2007**, *68*, 235−241.
(34) Zugenmaier, P. Conformation and Packing of various Crystalline Cellulose Fibers. *Prog. Polym. Sci.* **2001**, *26*, 1341−1417.
(35) Elguero, J.; Fruchier, A.; Pellegrin, V. Annular Tautomerism in the Solid State: a High Resolution N.M.R. Study. *J. Chem. Soc., Chem. Commun.* **1981**, 1207−1208.
(36) Goward, G. R.; Schuster, M. F. H.; Sebastiani, D.; Schnell, I.; Spiess, H. W. High-Resolution Solid-State NMR Studies of Imidazole-Based Proton Conductors: Structure Motifs and Chemical Exchange from 1H NMR. *J. Phys. Chem. B* **2002**, *106*, 9322−9334.
(37) Benhabbour, S. R.; Chapman, R. P.; Scharfenberger, G.; Meyer, W. H.; Goward, G. R. Study of Imidazole-Based Proton-Conducting Composite Materials Using Solid-State NMR. *Chem. Mater.* **2005**, *17*, 1605−1612.
(38) Fischbach, I.; Spiess, H. W.; Saalwächter, K.; Goward, G. R. Solid State NMR Spectroscopic Investigations of Model Compounds for Imidazole-Based Proton Conductors. *J. Phys. Chem. B* **2004**, *108*, 18500−18508.
(39) Hickman, B. S.; Mascal, M.; Titman, J. J.; Wood, I. G. Protonic Conduction in Imidazole: A Solid-State 15N NMR Study. *J. Am. Chem. Soc.* **1999**, *121*, 11486−11490.
(40) Diat, O.; Gebel, G. Fuel Cells: Proton Channels. *Nat. Mater.* **2008**, *7*, 13−14.
(41) Shenderovich, I. G.; Lesnichin, S. B.; Tu, C.; Silverman, D. N.; Tolstoy, P. M.; Denisov, G. S.; Limbach, H.-H. NMR Studies of Active-Site Properties of Human Carbonic Anhydrase II by Using 15N-Labeled 4-Methylimidazole as a Local Probe and Histidine Hydrogen-Bond Correlations. *Chem. - Eur. J.* **2015**, *21*, 2915−2929.
(42) Li, S.; Hong, M. Protonation, Tautomerization, and Rotameric Structure of Histidine: A Comprehensive Study by Magic-Angle-Spinning Solid-State NMR. *J. Am. Chem. Soc.* **2011**, *133*, 1534−1544.
(43) Hu, J.; Fu, R.; Nishimura, K.; Zhang, L.; Zhou, H.-X.; Busath, D. D.; Vijayvergiya, V.; Cross, T. A. Histidines, Heart of the Hydrogen Ion Channel from Influenza A Virus: Toward an Understanding of Conductance and Proton Selectivity. *Proc. Natl. Acad. Sci. U. S. A.* **2006**, *103*, 6865−6870.
(44) Isogai, A.; Usuda, M.; Kato, T.; Uryu, T.; Atalla, R. H. Solid-State CP/MAS Carbon-13 NMR Study of Cellulose Polymorphs. *Macromolecules* **1989**, *22*, 3168−3172.
(45) VanderHart, D. L.; Atalla, R. Studies of Microstructure in Native Celluloses using Solid-State Carbon-13 NMR. *Macromolecules* **1984**, *17*, 1465−1472.
(46) Evans, R.; Newman, R. H.; Roick, U. C.; Suckling, I. D.; Wallis, A. F. Changes in Cellulose Crystallinity during Kraft Pulping. Comparison of Infrared, X-ray Diffraction and Solid State NMR Results. *Holzforschung* **1995**, *49*, 498−504.
(47) Song, C.; Hu, K.-N.; Joo, C.-G.; Swager, T. M.; Griffin, R. G. TOTAPOL: a Biradical Polarizing Agent for Dynamic Nuclear Polarization Experiments in Aqueous Media. *J. Am. Chem. Soc.* **2006**, *128*, 11385−11390.
(48) Tobyn, M. J.; McCarthy, G. P.; Staniforth, J. N.; Edge, S. Physicochemical Comparison between Microcrystalline Cellulose and Cilicified Microcrystalline Cellulose. *Int. J. Pharm.* **1998**, *169*, 183−194.
(49) Zhao, L.; Li, W.; Plog, A.; Xu, Y.; Buntkowsky, G.; Gutmann, T.; Zhang, K. Multi-responsive Cellulose Nanocrystal-Rhodamine Conjugates: an Advanced Structure Study by Solid-State Dynamic Nuclear Polarization (DNP) NMR. *Phys. Chem. Chem. Phys.* **2014**, *16*, 26322−26329.
(50) Takahashi, H.; Lee, D.; Dubois, L.; Bardet, M.; Hediger, S.; De Paëpe, G. Rapid Natural-Abundance 2D 13C-13C Correlation Spectroscopy Using Dynamic Nuclear Polarization Enhanced Solid-State NMR and Matrix-Free Sample Preparation. *Angew. Chem.* **2012**, *124*, 11936−11939.
(51) Takahashi, H.; Hediger, S.; De Paëpe, G. Matrix-free Dynamic Nuclear Polarization enables Solid-State NMR 13C−13C Correlation Spectroscopy of Proteins at Natural Isotopic Abundance. *Chem. Commun.* **2013**, *49*, 9479−9481.
(52) Gibby, C. W.; Hall, J. XCIV.—The System Water−Chloroform. *J. Chem. Soc.* **1931**, *0*, 691−693.
(53) Lee, M.; Goldburg, W. I. Nuclear-Magnetic-Resonance Line Narrowing by a Rotating rf Field. *Phys. Rev.* **1965**, *140*, A1261−A1271.
(54) Bielecki, A.; Kolbert, A. C.; Levitt, M. H. Frequency-switched Pulse Sequences: Homonuclear Decoupling and dilute Spin NMR in Solids. *Chem. Phys. Lett.* **1989**, *155*, 341−346.
(55) Kuhn, L. T.; Akbey, Ü. *Hyperpolarization Methods in NMR Spectroscopy*; Springer, 2013; Vol. *338*.
(56) Metz, G.; Wu, X.; Smith, S. Ramped-Amplitude Cross Polarization in Magic-Angle-Spinning NMR. *J. Magn. Reson., Ser. A* **1994**, *110*, 219−227.
(57) Taylor, R. E. ^{13}C CP/MAS: Application to Glycine. *Concepts Magn. Reson.* **2004**, *22A*, 79−89.
(58) Bertani, P.; Raya, J.; Bechinger, B. 15N Chemical Shift Referencing in Solid State NMR. *Solid State Nucl. Magn. Reson.* **2014**, *61−62*, 15−18.
(59) van Rossum, B. J.; Boender, G. J.; de Groot, H. J. M. High Magnetic Field for Enhanced Proton Resolution in High-Speed CP/MAS Heteronuclear1H−13C Dipolar-Correlation Spectroscopy. *J. Magn. Reson., Ser. A* **1996**, *120*, 274−277.
(60) Munowitz, M. G.; Griffin, R. G. Two dimensional Nuclear Magnetic Resonance in Rotating Solids: An Analysis of Line Shapes in Chemical Shift Dipolar Spectra. *J. Chem. Phys.* **1982**, *76*, 2848−2858.
(61) Hong, M.; Fritzsching, K. J.; Williams, J. K. Hydrogen-Bonding Partner of the Proton-Conducting Histidine in the Influenza M2 Proton Channel revealed from 1H Chemical Shifts. *J. Am. Chem. Soc.* **2012**, *134*, 14753−14755.
(62) Li, S.; Su, Y.; Luo, W.; Hong, M. Water− Protein Interactions of an Arginine-Rich Membrane Peptide in Lipid Bilayers Investigated by Solid-State Nuclear Magnetic Resonance Spectroscopy. *J. Phys. Chem. B* **2010**, *114*, 4063−4069.
(63) Morcombe, C. R.; Paulson, E. K.; Gaponenko, V.; Byrd, R. A.; Zilm, K. W. 1H−15N Correlation Spectroscopy of Nanocrystalline Proteins. *J. Biomol. NMR* **2005**, *31*, 217−230.
(64) Hennig, J.; Limbach, H. H. Localization and Transfer of Protons between Nitrogen-15 Atoms of meso-Tetraphenylporphine probed by Nuclear Overhauser Effects and dipole-dipole Relaxation Times. *J. Am. Chem. Soc.* **1984**, *106*, 292−298.
(65) Schlabach, M.; Wehrle, B.; Rumpel, H.; Braun, J.; Scherer, G.; Limbach, H. H. NMR and NIR Studies of the Tautomerism of 5, 10, 15, 20-Tetraphenylporphyrin including Kinetic HH/HD/DD Isotope and Solid State Effects. *Ber. Bunsen-Ges. Phys. Chem.* **1992**, *96*, 821−833.
(66) Aguilar-Parrilla, F.; Claramunt, R. M.; Lopez, C.; Sanz, D.; Limbach, H.-H.; Elguero, J. High-Resolution Solid-State 13C and 15N NMR Spectroscopy of Pyrazole and 3, 5-Dimethylpyrazole adsorbed on Alumina and Silica. *J. Phys. Chem.* **1994**, *98*, 8752−8760.
(67) Braun, J.; Schwesinger, R.; Williams, P. G.; Morimoto, H.; Wemmer, D. E.; Limbach, H.-H. Kinetic H/D/T Isotope and Solid State Effects on the Tautomerism of the Conjugate Porphyrin Monoanion. *J. Am. Chem. Soc.* **1996**, *118*, 11101−11110.
(68) Klein, O.; Aguilar-Parrilla, F.; Lopez, J. M.; Jagerovic, N.; Elguero, J.; Limbach, H.-H. Dynamic NMR Study of the Mechanisms of Double, Triple, and Quadruple Proton and Deuteron Transfer in

DOI: 10.1021/acs.jpcc.6b07049
J. Phys. Chem. C 2016, 120, 19574−19585

Cyclic Hydrogen Bonded Solids of Pyrazole Derivatives. *J. Am. Chem. Soc.* **2004**, *126*, 11718−11732.
(69) Lopez, J. M.; Männle, F.; Wawer, I.; Buntkowsky, G.; Limbach, H. H. NMR Studies of double Proton Transfer in Hydrogen Bonded cyclic N,N ′-diarylformamidine Dimers: Conformational Control, Kinetic HH/HD/DD Isotope Effects and Tunneling. *Phys. Chem. Chem. Phys.* **2007**, *9*, 4498−4513.
(70) Lopez del Amo, J. M.; Langer, U.; Torres, V.; Buntkowsky, G.; Vieth, H.-M.; Pérez-Torralba, M.; Sanz, D. s.; Claramunt, R. M. a.; Elguero, J.; Limbach, H.-H. NMR Studies of Ultrafast Intramolecular Proton Tautomerism in Crystalline and Amorphous N, N′-Diphenyl-6-aminofulvene-1-aldimine: Solid-State, Kinetic Isotope, and Tunneling Effects. *J. Am. Chem. Soc.* **2008**, *130*, 8620−8632.
(71) Gedat, E.; Schreiber, A.; Albrecht, J.; Emmler, T.; Shenderovich, I.; Findenegg, G.; Limbach, H.-H.; Buntkowsky, G. 2H-Solid-State NMR Study of Benzene-d 6 Confined in Mesoporous Silica SBA-15. *J. Phys. Chem. B* **2002**, *106*, 1977−1984.
(72) de Sousa Amadeu, N.; Grünberg, B.; Frydel, J.; Werner, M.; Limbach, H.-H.; Breitzke, H.; Buntkowsky, G. Melting of Low Molecular Weight Compounds in Confinement Observed by 2H-Solid State NMR: Biphenyl, a Case Study. *Z. Phys. Chem.* **2012**, *226*, 1169−1186.
(73) Myhre, P.; Kruger, J.; Hammond, B.; Lok, S.; Yannoni, C.; Macho, V.; Limbach, H.; Vieth, H. Solid-State Carbon-13 CPMAS Spectra of rapidly equilibrating Carbocations. *J. Am. Chem. Soc.* **1984**, *106*, 6079−6080.
(74) Wehrle, B.; Zimmermann, H.; Limbach, H. H. A Solid-State Nitrogen-15 CPMAS NMR Study of Dye Tautomerism in glassy Polystyrene: Site Dependence of Double Minimum Potentials and their motional Averaging. *J. Am. Chem. Soc.* **1988**, *110*, 7014−7024.
(75) Foces-Foces, C.; Echevarría, A.; Jagerovic, N.; Alkorta, I.; Elguero, J.; Langer, U.; Klein, O.; Minguet-Bonvehí, M.; Limbach, H.-H. A Solid-State NMR, X-ray Diffraction, and ab initio Computational Study of Hydrogen-Bond Structure and Dynamics of Pyrazole-4-carboxylic Acid Chains. *J. Am. Chem. Soc.* **2001**, *123*, 7898−7906.
(76) Rössler, E.; Taupitz, M.; Börner, K.; Schulz, M.; Vieth, H. M. A simple Method analyzing 2H Nuclear Magnetic Resonance Line Shapes to determine the Activation Energy Distribution of mobile Guest Molecules in disordered Systems. *J. Chem. Phys.* **1990**, *92*, 5847−5855.
(77) Vyalikh, A.; Emmler, T.; Shenderovich, I.; Zeng, Y.; Findenegg, G. H.; Buntkowsky, G. H-2-Solid State NMR and DSC Study of Isobutyric Acid in mesoporous Silica Materials. *Phys. Chem. Chem. Phys.* **2007**, *9*, 2249−2257.
(78) Grünberg, B.; Grünberg, A.; Limbach, H. H.; Buntkowsky, G. Melting of Naphthalene Confined in Mesoporous Silica MCM-41. *Appl. Magn. Reson.* **2013**, *44*, 189−201.
(79) Limbach, H. H.; Denisov, G. S.; Shenderovich, I. G.; Tolstoy, P. M. Proton Tautomerism in Systems of Increasing Complexity: Examples from Organic Molecules to Enzymes. *Tautomerism: Concepts and Applications in Science and Technology* **2016**, 329−372.
(80) Gerritzen, D.; Limbach, H. H. Kinetic and Equilibrium Isotope Effects of Proton Exchange and Autoprotolysis of pure Methanol studied by Dynamic NMR Spectroscopy. *Ber. Bunsen-Ges. Phys. Chem.* **1981**, *85*, 527−535.
(81) Hearle, J. A fringed Fibril Theory of Structure in crystalline Polymers. *J. Polym. Sci.* **1958**, *28*, 432−435.
(82) Newman, R. H.; Davidson, T. C. Molecular Conformations at the Cellulose−Water Interface. *Cellulose* **2004**, *11*, 23−32.
(83) Kono, H.; Yunoki, S.; Shikano, T.; Fujiwara, M.; Erata, T.; Takai, M. CP/MAS 13C NMR Study of Cellulose and Cellulose Derivatives. 1. Complete Assignment of the CP/MAS 13C NMR Spectrum of the native Cellulose. *J. Am. Chem. Soc.* **2002**, *124*, 7506−7511.
(84) Afeworki, M.; Vega, S.; Schaefer, J. Direct Electron-to-Carbon Polarization Transfer in homogeneously doped Polycarbonates. *Macromolecules* **1992**, *25*, 4100−4105.
(85) van der Wel, P. C.; Hu, K.-N.; Lewandowski, J.; Griffin, R. G. Dynamic Nuclear Polarization of amyloidogenic Peptide Nanocrystals: GNNQQNY, a Core Segment of the Yeast Prion Protein Sup35p. *J. Am. Chem. Soc.* **2006**, *128*, 10840−10846.
(86) Dementyev, A.; Cory, D.; Ramanathan, C. Dynamic Nuclear Polarization in Silicon Microparticles. *Phys. Rev. Lett.* **2008**, *100*, 127601.
(87) Lafon, O.; Rosay, M.; Aussenac, F.; Lu, X.; Trébosc, J.; Cristini, O.; Kinowski, C.; Touati, N.; Vezin, H.; Amoureux, J. P. Beyond the Silica Surface by Direct Silicon-29 Dynamic Nuclear Polarization. *Angew. Chem., Int. Ed.* **2011**, *50*, 8367−8370.
(88) Kalk, A.; Berendsen, H. Proton Magnetic Relaxation and Spin Diffusion in Proteins. *J. Magn. Reson.* **1976**, *24*, 343−366.

DOI: 10.1021/acs.jpcc.6b07049
J. Phys. Chem. C 2016, 120, 19574−19585